Research Square

Preprints are preliminary reports that have not undergone peer review.
They should not be considered conclusive, used to inform clinical practice,
or referenced by the media as validated information.

Decellularized Human Amnion-Chorion Membrane as a Novel Scaffold for Expansion of Human Umbilical Cord Tissue- Derived Mesenchymal Stem Cells and Production of Chlorogenic Acid-Loaded Extracellular Vesicles Against Glioblastoma

Jaseem Batchaa[1]

jaseemislam20@gmail.com

Acadicell Innovations International Pvt. Ltd

Raghu Babu Pothireddy[1]

Acadicell Innovations International Pvt. Ltd

Praveen Kumar L[1]

Acadicell Innovations International Pvt. Ltd

Research Article

Keywords: Glioblastoma, Extracellular vesicles, Mesenchymal stem cells, Chlorogenic acid, Decellularized amnion-chorion membrane, Freeze-thaw decellularization, EGFR, Network pharmacology

Posted Date: November 4th, 2026

DOI: https://doi.org/10.21203/rs.3.rs-11222166/v1

License: This work is licensed under a Creative Commons Attribution 4.0 International License.
Read Full License

Additional Declarations: No competing interests reported.

Decellularized Human Amnion-Chorion Membrane as a Novel Scaffold for Expansion of Human Umbilical Cord Tissue-Derived Mesenchymal Stem Cells and Production of Chlorogenic Acid-Loaded Extracellular Vesicles Against Glioblastoma

Jaseem Batchaa[1]*, Raghu Babu Pothireddy[1], Praveen Kumar L[1]

[1]*Department of Stem Cell Biology, Acadicell Innovations International Pvt. Ltd, Vandalur, Chennai, Tamil Nadu, India.*

***Corresponding author:** Jaseem Batchaa. Email: jaseemislam20@gmail.com*

Abstract

Background: Brain cancer named glioblastoma multiforme often called GBM is hard to manage. Survival tends to stretch just 14 to 16 months, despite aggressive therapies. Research now turns toward tiny bubbles released by mesenchymal stem cells, known as extracellular vesicles. These particles slip through the blood-brain barrier without trouble. Meanwhile, attention grows around caffeic acid, a substance found in plants. Early findings hint it may slow tumor growth in the brain. Yet issues remain. Poor absorption into tissues marks one limitation, while access to the brain proves especially difficult. A new approach emerges here. In this study, a biological layer decellularized human amnion-chorion membrane, known as dHACM was tested to cultivate stem cells from umbilical cords, labeled hUCT-MSCs. From these, extracellular vesicles form, capable of transporting CGA against aggressive brain tumors like glioblastoma multiforme. From dHACM tissue, MSCs were isolated through a targeted technique, afterward verifying cell identity with precision. Flow cytometry joined karyotyping in confirming traits, ensuring accuracy without reliance on assumptions. Extracellular vesicles emerged from these cultured cells, captured for further study. Nanoparticle tracking analysis, along with transmission electron microscopy, revealed their physical details clearly. Microwave-assisted loading was applied to insert CGA into the vesicles successfully. Each phase unfolded systematically, maintaining alignment with initial design goals. Moreover, network pharmacology was applied alongside molecular docking to explore how CGA behaves. It turned out EGFR was a key target of CGA activity. When examining U87 glioblastoma multiforme cells, both EVs and CGA showed measurable effects. Health status of the hUCT-MSCs remained strong throughout testing. Abundant levels of CD90 and CD105 appeared in the sample, yet CD31 remained low. Viability was confirmed through standard measures. With particles falling within expected dimensions, binding between CGA and EGFR occurred exactly as intended. Exposure to U87 cells revealed growth inhibition by CGA alone; effects intensified once EVs entered the mix. Findings highlight freeze-thawed dHACM supports MSC expansion, enabling production of EVs capable of delivering CGA against glioblastoma multiforme. Natural compounds like this may one day play a role in targeting aggressive brain tumors. A single advance, but meaningful.

Keywords: Glioblastoma; Extracellular vesicles; Mesenchymal stem cells; Chlorogenic acid; Decellularized amnion-chorion membrane; Freeze-thaw decellularization; EGFR; Network pharmacology

1. Introduction

A deadly form of brain cancer, glioblastoma multiforme (GBM; WHO Grade IV), strikes more adults than any other primary malignant type, making up roughly 14.3% of cases[1]. Even with intensive treatment , surgery followed by temozolomide and radiation ,the average lifespan after diagnosis stretches only 14 to 16 months, while fewer than 5 out of every 100 survive five years[1]. Because of the blood-brain barrier, diverse tumor cells, and growing resistance to drugs, medicines often fail to work well[2].

Among extracellular vesicles, those ranging from 30 to 150 nanometers, especially exosomes have drawn increasing attention due to their ability to traverse the blood-brain barrier while carrying treatments into brain tumor areas[2]. Rather than relying on synthetic systems, these naturally occurring carriers show compatibility with biological processes. Originating from mesenchymal stem cells, they display a tendency to migrate toward tumors, guided by intrinsic signals[8]. Their contents also influence immune responses, adding another layer of potential benefit. In support of earlier findings, an analysis published in 2024 documented consistent suppression of glioblastoma growth using such vesicles across various animal studies[9].

Human umbilical cord tissue-derived mesenchymal stem cells offer a widely accepted, fast-growing cell option. A new method using frozen then thawed human amniotic membrane may support their growth better. Ice crystals form during temperature shifts, breaking open donor cells but leaving behind structural fibers, natural signals, and active molecules intact. This approach skips harsh cleaning chemicals, avoiding harmful leftovers linked to traditional processing techniques.

Though present in coffee and green tea, CGA faces challenges due to its brief presence in blood , lasting just over an hour and poor access to the brain. Early results from a 2023 study show it can be safely used in patients with aggressive glioma, hinting at possible benefits. Because of these pharmacokinetic barriers, researchers have turned to extracellular vesicles as a smarter way to carry the compound where needed.

This appears to be the initial investigation using freeze-thaw dHACM as a support structure for growing hUCT-MSCs aimed at EV-driven treatment of glioblastoma. Computational modeling comes into play alongside virtual binding predictions. Laboratory tests add functional validation within one unified framework. While earlier efforts explored similar cells, none combined these methods directly targeting brain tumors. The approach links tissue engineering with therapeutic vesicle production through deliberate design. Such integration has not been reported under these exact conditions before. The overall experimental workflow is summarized in Figure 1.

2. Materials and Methods

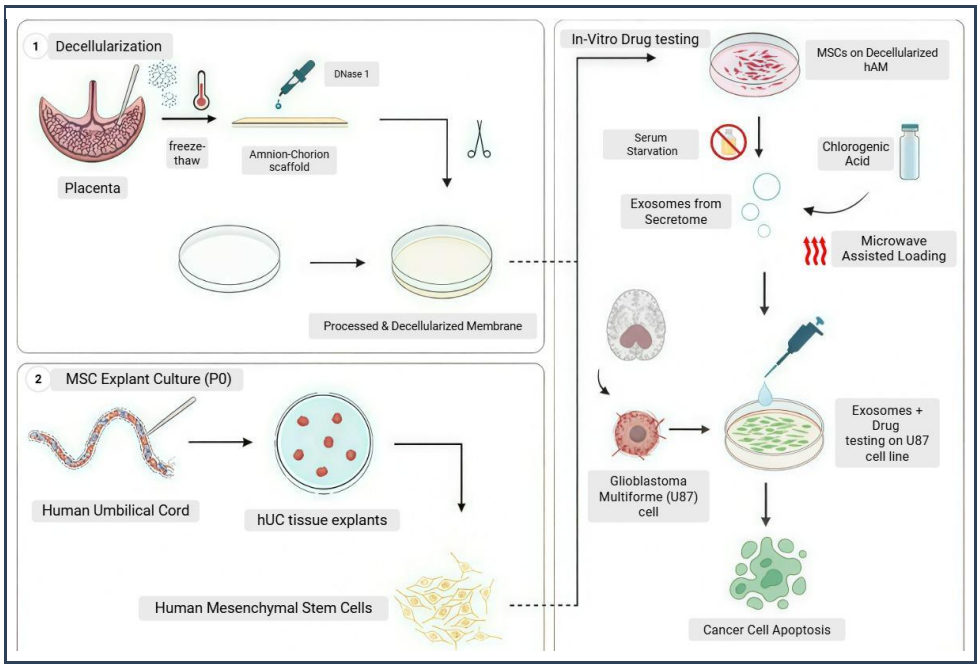


Figure 1. *Diagrammatic overview of the study workflow.*

2.1 Freeze-Thaw Decellularization of Human Amnion-Chorion Membrane

From patients who agreed to donate after planned C-sections, human placental tissues were collected under approved ethics guidelines. Once isolated, the amnion and chorion were carefully rinsed repeatedly with phosphate-buffered saline to clear away blood remnants and loose cells. Instead of chemical agents, a cycle of deep freezing and slow warming broke open cells: three rounds occurred, each involving 24 hours frozen at minus 80 degrees Celsius then half an hour thawing at body temperature. Ice crystals formed during these shifts damaged cell structures but left behind the natural extracellular matrix intact the weave of collagen fibers plus signaling molecules stayed functional, free from toxic leftovers. Afterward, washes resumed, now including sterilized buffers mixed with antimicrobial additives; finally, materials rested refrigerated at four degrees Celsius until experiments began.

Translucent tissue replaced the original opaque look after treatment, showing progress (Figure 2). Visual checks under magnification revealed structural changes in the matrix (Figures 3-4). What remained matched expected patterns once cells were removed (Figure 5). Evidence across methods supported effective removal. Each image set contributed to confirming results.

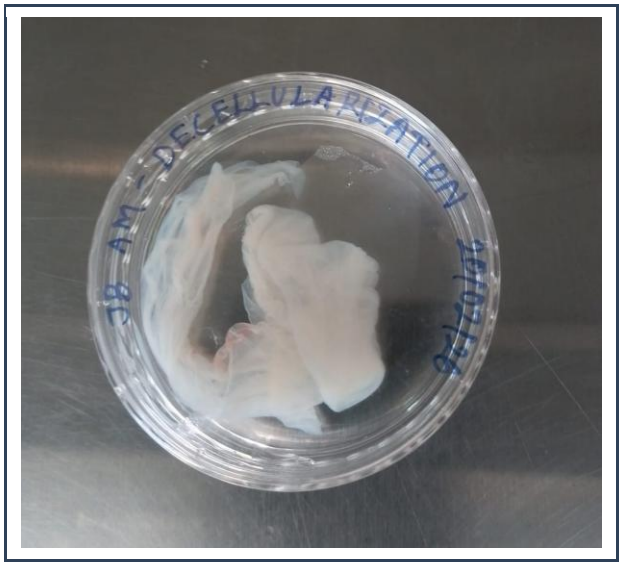


Figure 2. *Gross photograph of dHACM — post-decellularization*

Looking at the amnion-chorion under a microscope before and after removing cells appears in Figure 2. Intact single-layered epithelium, complete with visible nuclei above the stroma, marks the natural state seen in Figure 3 , this sets the baseline. Once subjected to freezing and thawing, structural breakdown becomes evident: epithelial organization collapses, tissue fragments scatter (Figure 4). What remains aligns with effective cell elimination, yet fibrous extracellular matrix elements persist[4][11].



Figure 3. *Histological cross-section of native (non-decellularized) human amnion-chorion membrane showing an intact, continuous epithelial layer with visible nuclear profiles overlying the stromal compartment. This serves as the pre-decellularization control.*

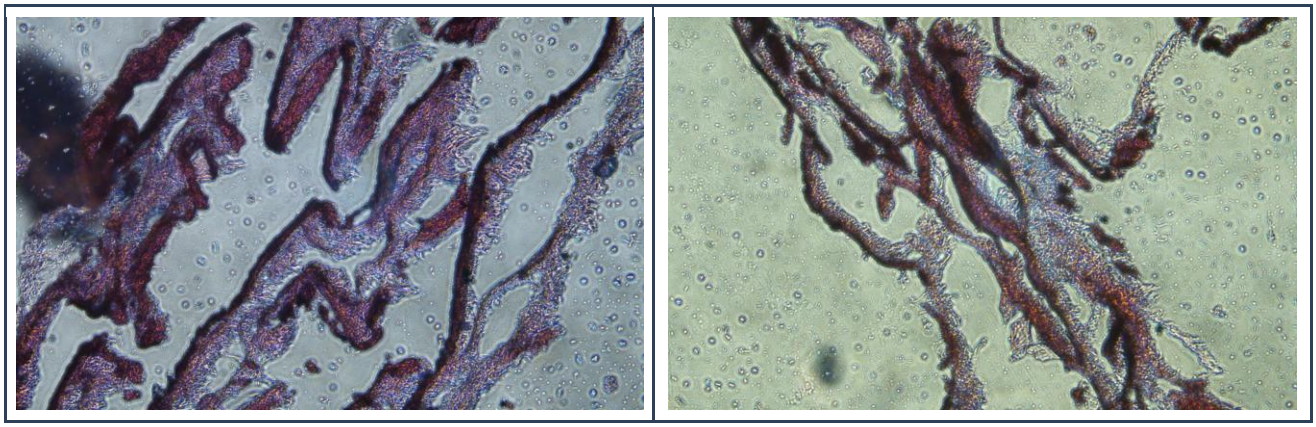


Figure 4. *Post-decellularization histological assessment of dHACM following freeze-thaw cycling. The organized epithelial architecture is absent; the fragmented, acellular ECM pattern indicates successful removal of cellular content, with residual fibrous ECM material retained.*

Across several areas of the dHACM scaffold (Figure 4), light microscopy showed a retained collagen structure made up of tangled ECM fibers, indicating the extracellular matrix kept its form after freeze-thaw decellularization[11].

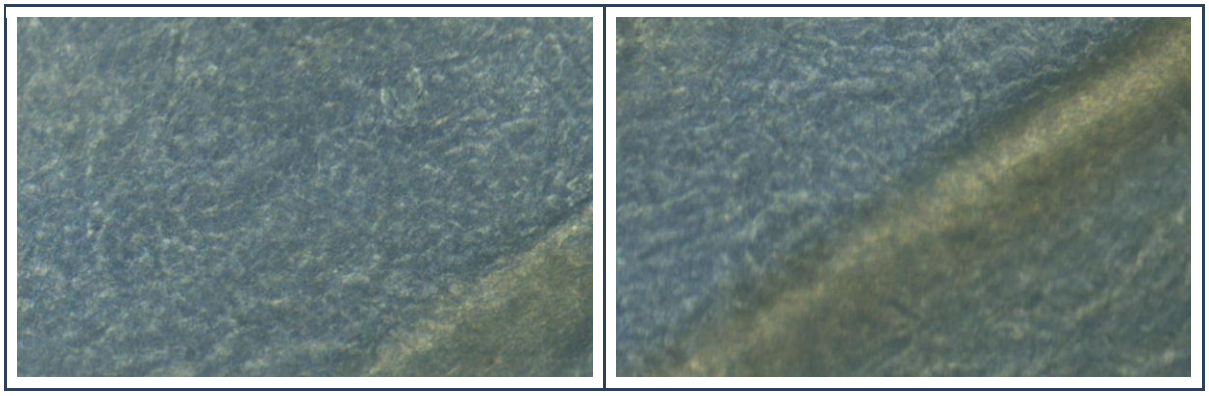


Figure 5. *Light micrograph of freeze-thaw dHACM showing the preserved collagen fibrillar network. Wavy, interwoven ECM fibers are clearly visible, confirming structural integrity of the scaffold post-decellularization.*

2.2 Isolation and Explant Culture of hUCT-MSCs on dHACM

From umbilical cord pieces, Wharton's jelly was carefully removed using sterile methods, then cut into small sections about 2–3 mm³ in size before being placed on culture containers[10].Instead of immediate growth, cultures stayed in α-MEM medium , supplied by Gibco with added fetal bovine serum (10%) and antimicrobial mix (1%) under warm, controlled atmosphere (37°C with 5% CO_2). Fresh nutrients arrived every three days, replacing old fluid until mesenchymal stem cells began spreading outward. Once coverage reached between 80% and 90%, detachment occurred via 0.25% trypsin-EDTA treatment; afterward, expansion continued on modified dHACM layers to study attachment efficiency. Observation through phase-based imaging tracked changes in shape and migration throughout development phases (Figures 6-8).

2.3 Characterization of hUCT-MSCs

2.3.1 Flow Cytometry. Some 4,900 or more events per marker were captured using correct isotype settings. Passage 2 saw hUCT-MSCs labeled with FITC-tagged anti-CD105, alongside FITC-linked anti-CD90, while PE-marked anti-CD31 was included - viability checked via 7-AAD staining[15].

2.3.2 Karyotyping. Chromosomal stability was assessed by conventional G-banding karyotyping at an accredited cytogenetics facility, reported per ISCN nomenclature.

2.4 EV Isolation and Characterization

From hUCT-MSCs that had gone without serum for two days, liquid was taken after spinning it down twice - first gently, then harder to clear out whole cells and leftover fragments. Following this, tiny particles known as EVs were pulled out using a polymer method, brought back into solution with buffer fluid, then kept frozen below zero degrees Celsius [5]. Their sizes and how many there were showed up clearly through light-scattering analysis on a NanoSight tool. Shape and structure received confirmation under an electron microscope set to thirty thousand times zoom, powered at two hundred kilovolts [5].

2.5 Microwave-Assisted Loading of Chlorogenic Acid into EVs

CGA (Sigma-Aldrich) was dissolved in DMSO and diluted in PBS. EV-CGA complexes were prepared by microwave-assisted loading using optimized pulse parameters to facilitate transient membrane permeabilization and drug encapsulation. Unencapsulated CGA was removed by size-exclusion filtration. Two loading concentrations were evaluated: EV+CGA 30 μg and EV+CGA 40 μg.

2.6 Network Pharmacology and Molecular Docking

From SwissTargetPrediction and PharmMapper came the CGA targets; meanwhile, data on GBM-linked genes emerged via GeneCards, DisGeNET, and OMIM. Shared gene sets then entered protein interaction mapping through STRING paired with Cytoscape [6]. The EGFR model, sourced as PDB ID 1IVO, along with CGA molecule (PubChem CID: 1794427), underwent preparation before molecular docking ran in AutoDock Vina. Final views of atomic contacts appeared using PyMOL together with BIOVIA Discovery Studio [7].

2.7 MTT Cytotoxicity Assay

U87 GBM cells (5×10^3/well, 96-well plate) were treated with CGA at 10, 20, 40, 80, and 160 μg/mL for 48 h in triplicate. MTT reagent was added (4 h at 37°C), formazan dissolved in DMSO, and absorbance measured at 570 nm. Cell survival and inhibition rates were calculated as: Cell Survival Rate (%) = (ODSample − ODBlank) / (ODControl − ODBlank) × 100; $IC_{50} = x_1 + (50 - y_1)(x_2 - x_1)/(y_2 - y_1)$.

2.8 Scratch Wound-Healing Assay

Confluent U87 cells were scratched with a 200 μL pipette tip, washed with PBS, and treated with: (i) Control, (ii) Naked EVs (nEVs), (iii) Free CGA (fDrug), (iv) EV+CGA 30 μg, and (v) EV+CGA 40 μg. Phase-contrast images were captured at 0 h and 24 h; wound width was measured using ImageJ software and % wound closure calculated.

2.9 Statistical Analysis

Each experiment ran three times. Results show average values alongside standard deviation. For analysis, one-way ANOVA followed by Tukey's method handled comparisons; significance set at p less than 0.05 using GraphPad Prism version 9.0.

3. Results

3.1 Freeze-Thaw Decellularization and dHACM ECM Characterization

After three rounds of freezing and thawing, the amnion-chorion tissue shifted visibly, going from pink and cloudy to clear (Figure 2), which matches what is expected when cells are effectively removed.[4] Under light magnification (Figures 4–5), the collagen structure remained dense and well-organized throughout various parts of the scaffold, showing that the process did not disrupt its natural layout [11]. Because the fibrous framework stays in place, it offers physical and chemical signals helpful for MSC attachment and signaling functions [12]. Unlike methods using SDS, this technique sidesteps leftover harsh chemicals, resulting in a more biocompatible base for growing cells [16].

3.2 hUCT-MSC Isolation, Expansion, and Morphological Assessment

From days five through seven onward, spindle-shaped cells resembling fibroblasts emerged when Wharton's jelly tissue was cultured on tissue coated plates [10]. Instead of dense clusters at first, phase-contrast imaging captured scattered cell migration beginning at the explant border (Figure 6). Gradually, these areas expanded into patchy layers where swirling arrangements became noticeable. By later stages, uniform sheets formed across regular culture surfaces (Figure 7). When grown atop dHACM(Figure 8), MSCs took on longer, star-like shapes - different from those seen under standard conditions. This shift likely resulted from physical cues embedded within the scaffold's fiber network guiding directional growth.

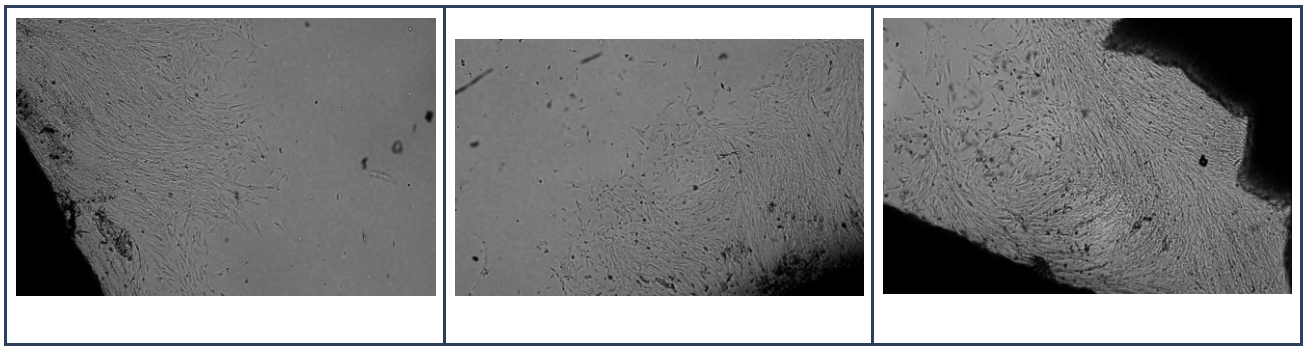


Figure 6. *Phase-contrast micrograph of hUCT-MSC early explant outgrowth (P0) from Wharton's jelly tissue seeded on standard tissue culture-treated plates.*

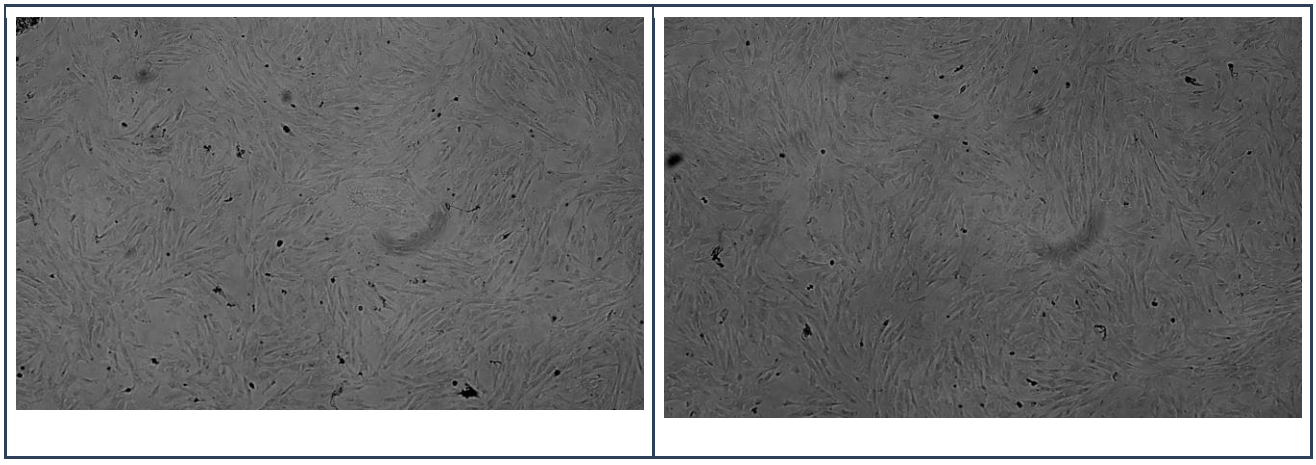


Figure 7. *Phase-contrast micrograph of hUCT-MSCs at Passage 1 on standard tissue culture-treated plates showing confluent monolayer with characteristic spindle-shaped morphology and whorling arrangement.*

Upon passaging onto standard tissue culture-treated plates, hUCT-MSCs maintained their characteristic fibroblastic morphology and proliferative capacity across successive passages, with sustained whorling monolayer organization (Figure 7).

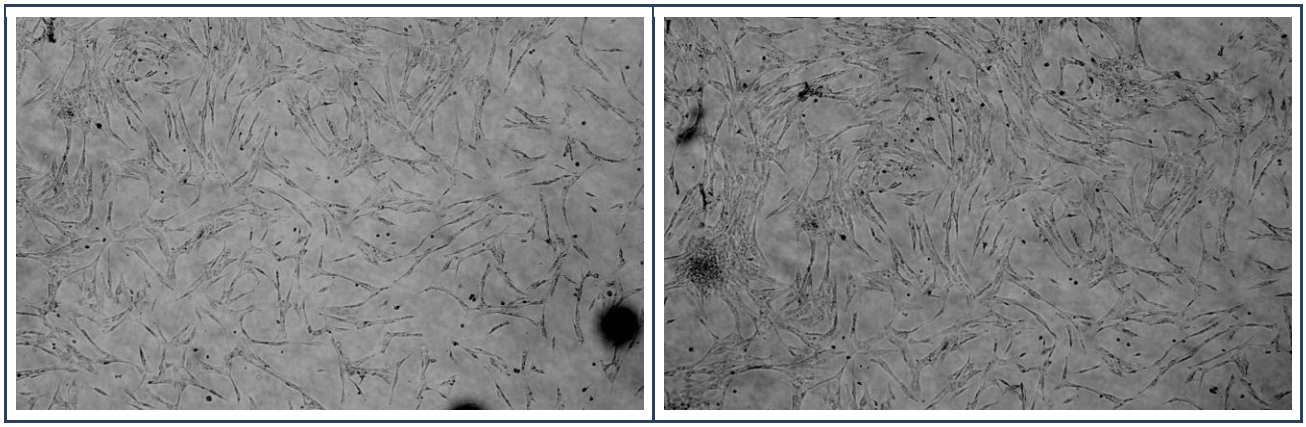


Figure 8. *Phase-contrast micrograph of hUCT-MSCs growing on decellularized hACM (dHACM) scaffold surface. Cells exhibit elongated, stellate morphology with extended cytoplasmic projections, reflecting contact guidance from the underlying ECM fibrillar topography of the dHACM scaffold.*

Cells grown on dHACM stuck well, multiplied steadily; their shape shifted subtly longer, star-like, unlike those on regular plates. This change likely followed cues from the collagen fibers beneath, part of the ECM's structure shown in Figure 8 [12].

Passage 2 samples, analyzed via flow cytometry, showed traits matching ISCT standards for MSCs [15]. CD105 appeared in 95.3% of cells; similarly, CD90 reached 91.7%. In contrast, CD31 levels stayed low , only 1.33%. Most cells remained viable: 98.6%, measured by lack of 7-AAD uptake. Data appear in Figure 9 and Table 1.

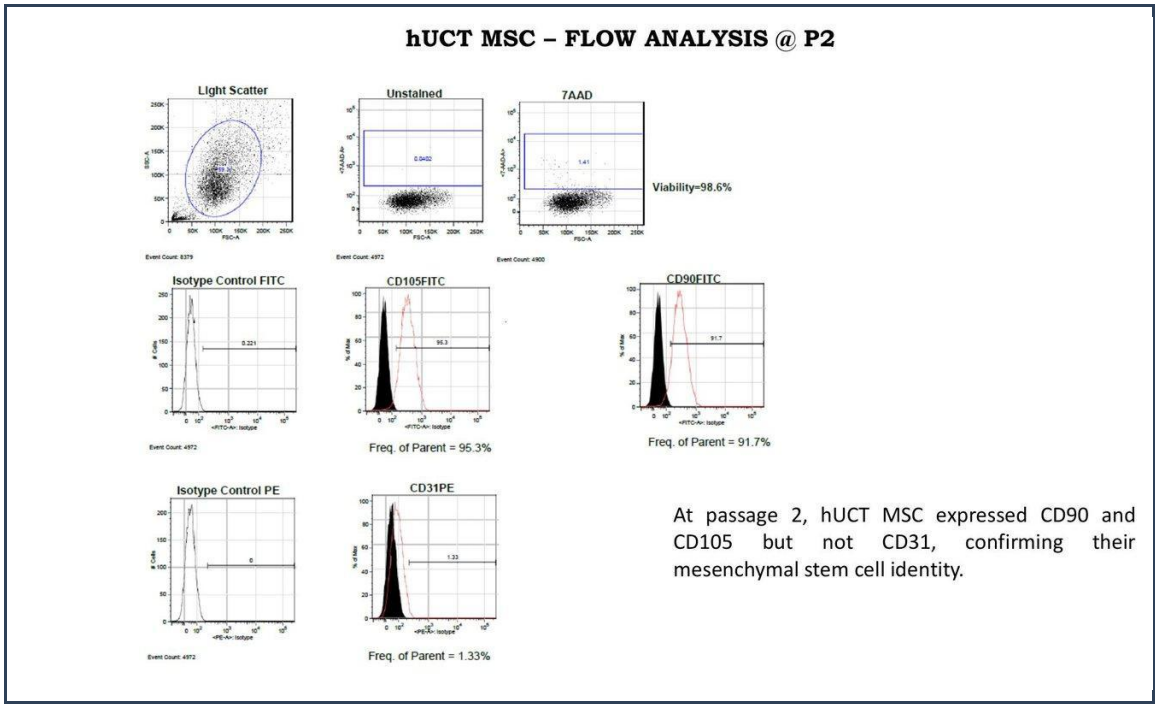


Figure 9. *Flow cytometric characterization of hUCT-MSCs at Passage 2. Cells expressed MSC-positive markers CD105 (95.3%) and CD90 (91.7%) while being negative for endothelial marker CD31 (1.33%). Cell viability by 7-AAD exclusion was 98.6%, confirming high-quality MSC preparation.*

Table 1. Flow cytometric characterization of hUCT-MSCs at passage 2.

Marker	Expression Type	Frequency of Parent (%)	Interpretation
CD105 (FITC)	Positive	95.3%	MSC marker — positive
CD90 (FITC)	Positive	91.7%	MSC marker — positive
CD31 (PE)	Negative	1.33%	Endothelial — negative
7-AAD	Viability	98.6%	High viability confirmed

3.3 Karyotyping

Chromosome structure appeared typical during metaphase, showing a standard male pattern (46,XY) without irregular changes (Figure 10). This outcome supports stable genetics in the growing hUCT-MSC group, an essential checkpoint before medical use.

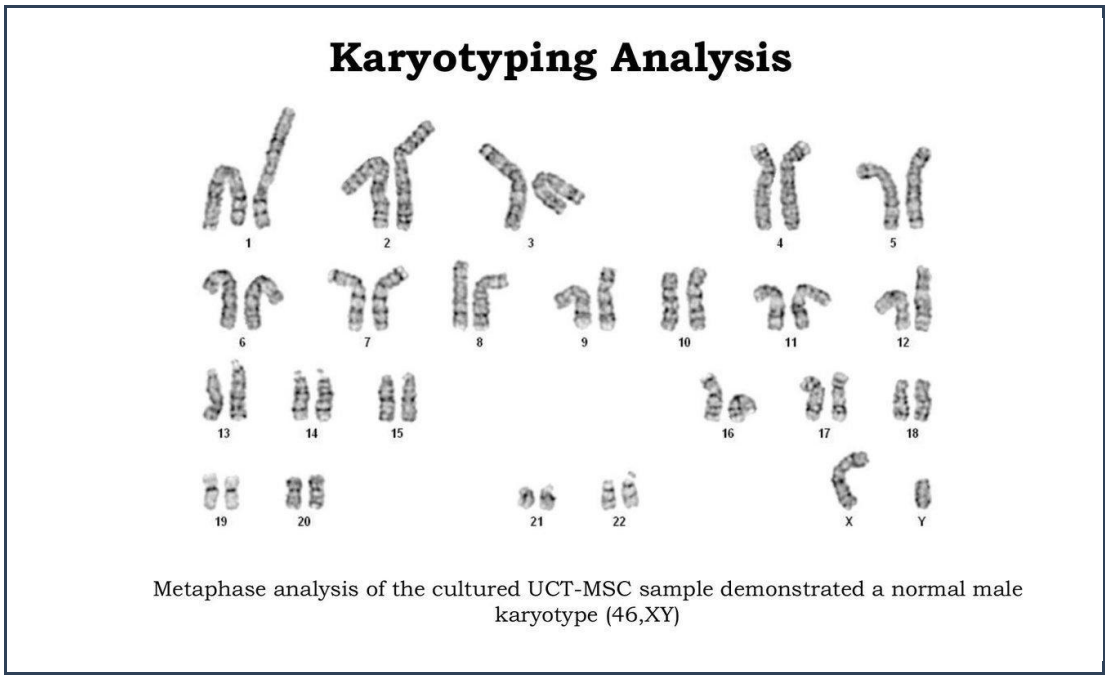


Figure 10. *Karyotyping analysis of hUCT-MSCs. G-banding confirmed a normal male karyotype (46,XY) with no structural rearrangements or numerical abnormalities, confirming genomic stability of the expanded MSC population.*

3.4 EV Characterization — NTA and TEM

Among detected particles, most appeared around 113.1 nanometers, making up nearly 92 percent. This group showed a spread of about 113.5 nm across its base. A smaller cluster emerged near 244.2 nanometers, accounting for just over eight percent. When ranked by size, half fell above and half below 119.3 nm, varying widely with a standard deviation close to 79 nm. Such dimensions align loosely with what is expected for exosomes under current standards. Particle density began at one quadrillion per milliliter before analysis. These results are shown in Figure 11 and summarized in Table 2.

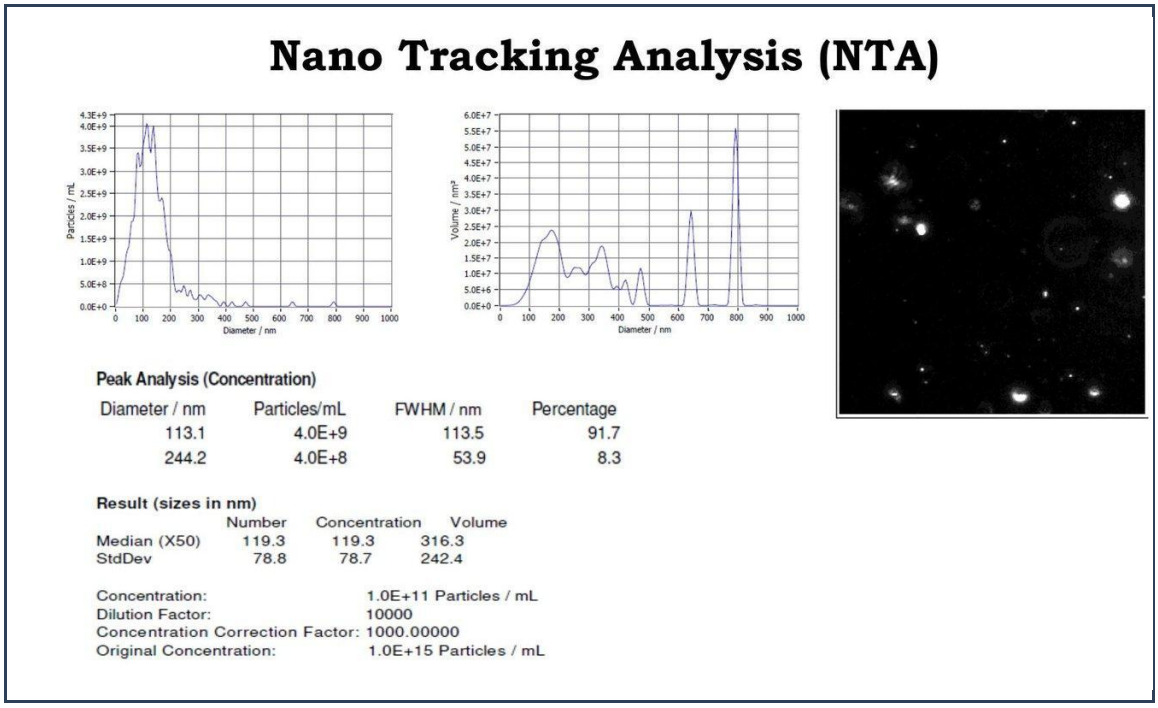


Figure 11. *Nanoparticle Tracking Analysis (NTA) of hUCT-MSC-derived EVs. Left: particle size distribution showing dominant peak at 113.1 nm (91.7%). Middle: volume distribution. Right: representative NanoSight field image of EVs in suspension.*

Table 2. NTA size distribution summary of hUCT-MSC-derived EVs.

Parameter	Number	Concentration	Volume
Median X50 (nm)	119.3	119.3	316.3
Std Dev (nm)	78.8	78.7	242.4
Peak 1 diam. (nm)	113.1 (91.7%)	—	—
Peak 2 diam. (nm)	244.2 (8.3%)	—	—
Concentration	1.0×10^{15} /mL	—	—

TEM at 30,000× confirmed round to oval membrane-bound vesicles with characteristic EV morphology and sizes consistent with the exosomal range (Figure 12) [5].

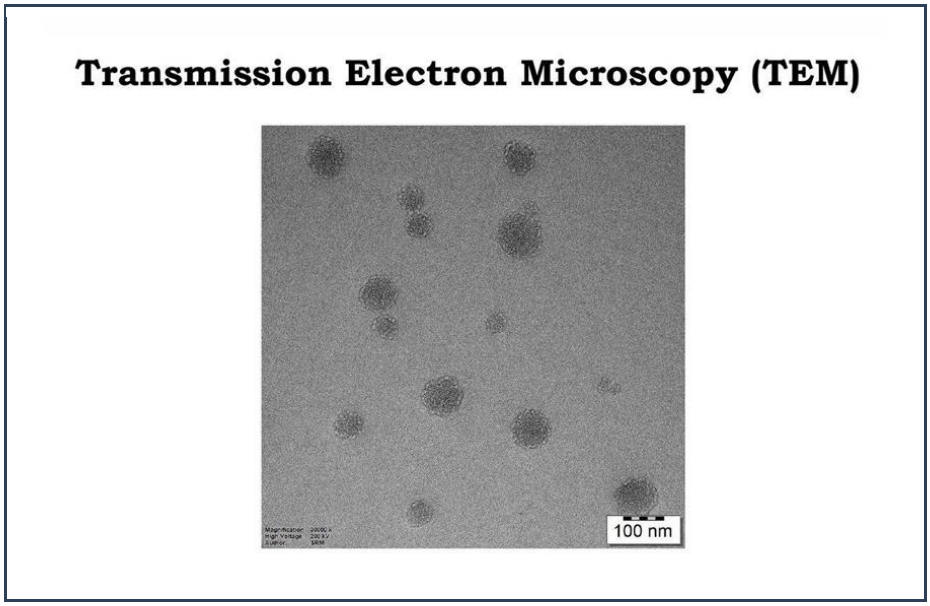


Figure 12. *Transmission Electron Microscopy (TEM) of hUCT-MSC-derived EVs at 30,000× magnification (200 kV). Spherical, membrane-bound vesicular structures of exosomal size range are clearly visible.*

3.5 Network Pharmacology — Hub Target Identification

Nine central hub targets were found where CGA effects meet GBM disease mechanisms - EGFR, MAPK1, MMP2, SRC, CASP8, PRKCD, HDAC1, HDAC2, and MMP14 as shown in Figure 13 [6]. With the strongest network links, EGFR and SRC stood out. Pathway analysis through KEGG pointed to PI3K-Akt, MAPK, and apoptosis routes[13], shaping the choice of EGFR for focused docking studies.

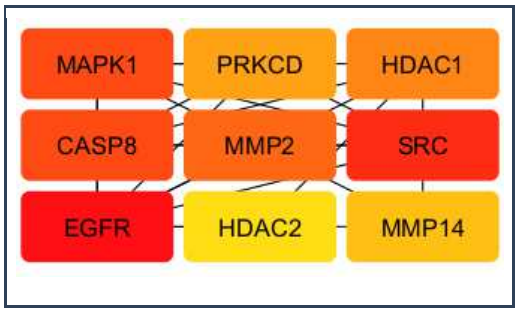


Figure 13. *Protein-protein interaction (PPI) hub network of key molecular targets at the intersection of chlorogenic acid pharmacology and GBM pathophysiology.*

3.6 Molecular Docking of CGA with EGFR

Docking CGA into the ATP-binding site of the EGFR kinase domain showed hydrogen bonds forming at MET769, GLQ767, and ASP831 (Figure 14) [7]. With these positions involved in how ligands bind during inhibition, interference similar to established drugs seems likely [7]. In separate studies on solid tumors, blocking the EGFR/p-Akt/Snail pathway by CGA appeared consistently observed [14].

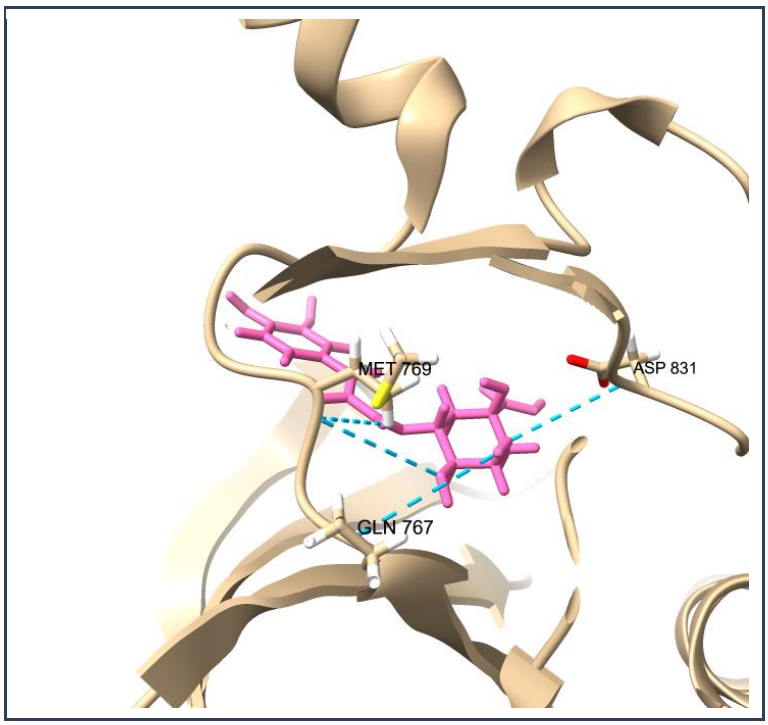
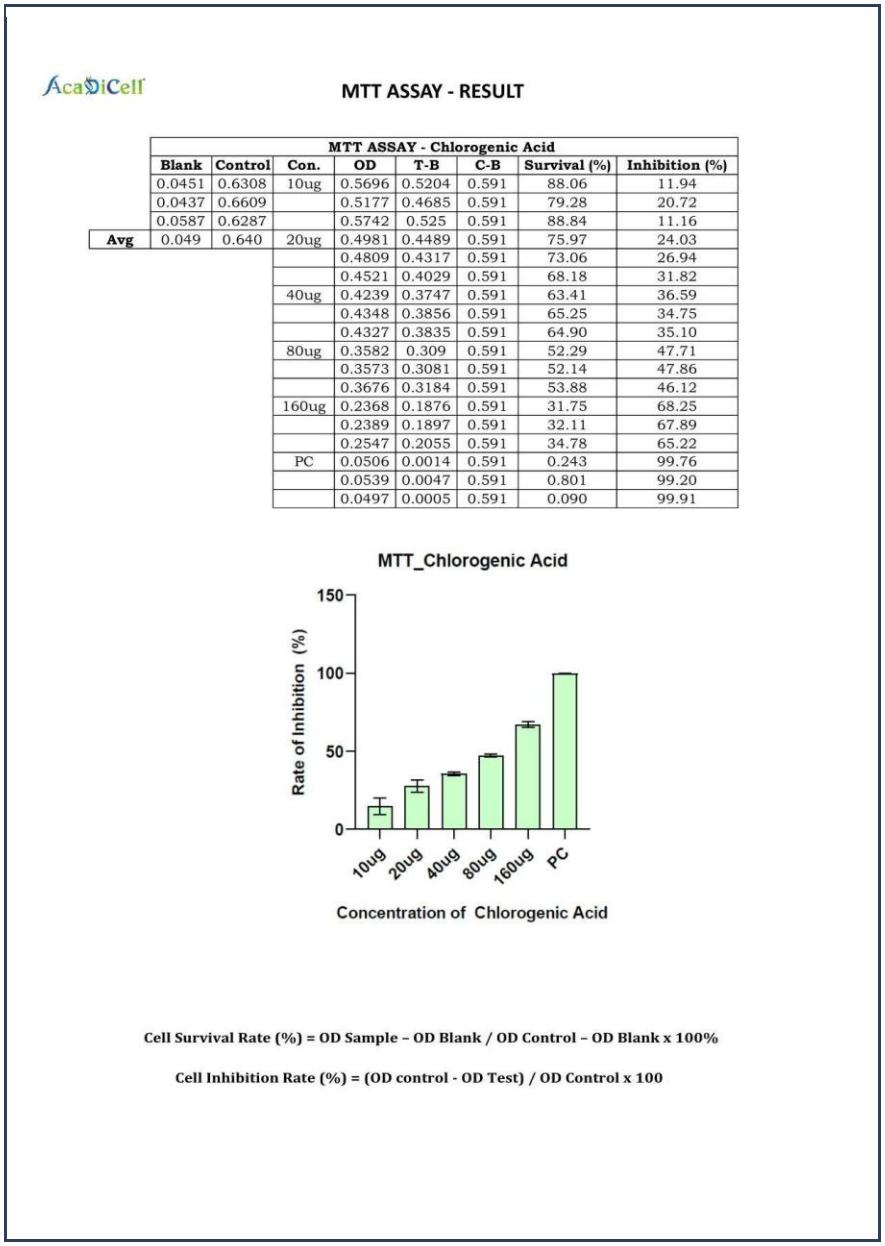


Figure 14. *Molecular docking of chlorogenic acid within the EGFR kinase domain ATP-binding pocket.*

3.7 MTT Cytotoxicity Assay

Free CGA demonstrated clear dose-dependent cytotoxicity against U87 GBM cells (Figures 15-16, Table 3). Inhibition increased from 14.60% at 10 µg to 67.12% at 160 µg, with an IC_{50} of 91.15 µg. These findings align with published reports of CGA anti-proliferative activity in glioblastoma models[13] and the Phase I clinical trial confirming anti-tumor activity in recurrent glioma patients [3].



AcaDiCell

MTT ASSAY - RESULT

	MTT ASSAY - Chlorogenic Acid							
	Blank	Control	Con.	OD	T-B	C-B	Survival (%)	Inhibition (%)
	0.0451	0.6308	10ug	0.5696	0.5204	0.591	88.06	11.94
	0.0437	0.6609		0.5177	0.4685	0.591	79.28	20.72
	0.0587	0.6287		0.5742	0.525	0.591	88.84	11.16
Avg	0.049	0.640	20ug	0.4981	0.4489	0.591	75.97	24.03
				0.4809	0.4317	0.591	73.06	26.94
				0.4521	0.4029	0.591	68.18	31.82
			40ug	0.4239	0.3747	0.591	63.41	36.59
				0.4348	0.3856	0.591	65.25	34.75
				0.4327	0.3835	0.591	64.90	35.10
			80ug	0.3582	0.309	0.591	52.29	47.71
				0.3573	0.3081	0.591	52.14	47.86
				0.3676	0.3184	0.591	53.88	46.12
			160ug	0.2368	0.1876	0.591	31.75	68.25
				0.2389	0.1897	0.591	32.11	67.89
				0.2547	0.2055	0.591	34.78	65.22
			PC	0.0506	0.0014	0.591	0.243	99.76
				0.0539	0.0047	0.591	0.801	99.20
				0.0497	0.0005	0.591	0.090	99.91

Cell Survival Rate (%) = OD Sample – OD Blank / OD Control – OD Blank x 100%

Cell Inhibition Rate (%) = (OD control - OD Test) / OD Control x 100

Figure 15. *MTT assay raw data sheet for chlorogenic acid on U87 GBM cells.*

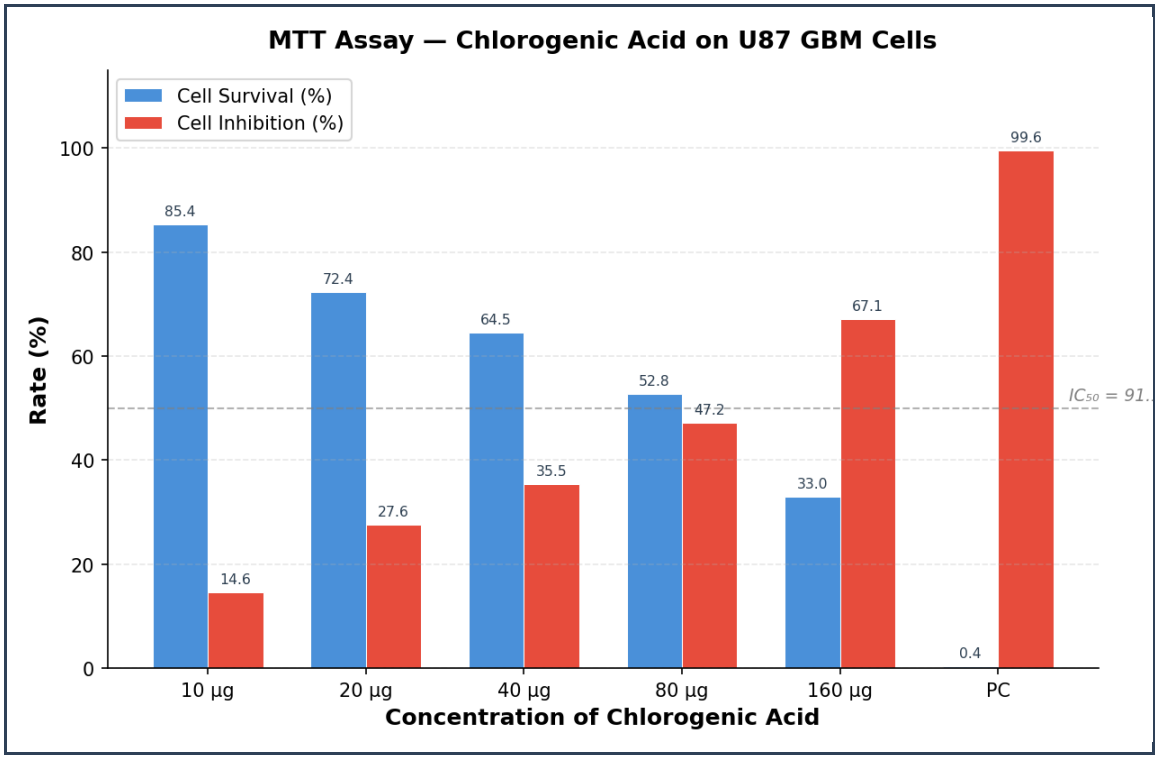


Figure 16. *MTT assay - dose-dependent Cell Survival (%) and Cell Inhibition (%) of U87 GBM cells treated with chlorogenic acid at concentrations of 10–160 µg. IC_{50} = 91.15 µg.*

Table 3. MTT assay - dose-dependent inhibition of U87 GBM cells by chlorogenic acid.

Concentration	Mean OD	T–B	C–B	Survival (%)	Inhibition (%)
10 µg	0.553	0.504	0.591	85.39	14.60
20 µg	0.477	0.428	0.591	72.40	27.60
40 µg	0.430	0.381	0.591	64.52	35.48
80 µg	0.361	0.312	0.591	52.77	47.23
160 µg	0.243	0.194	0.591	32.96	67.12
PC	0.051	0.002	0.591	0.38	99.62

Avg Blank = 0.049; Avg Control = 0.640; IC_{50} = 91.15 µg. T = Treated; B = Blank; C = Control; PC = Positive Control.

3.8 Scratch Wound-Healing Assay

EV-encapsulated CGA significantly suppressed U87 GBM cell migration (Figures 17-18, Table 4). The untreated control exhibited 55.12% wound closure at 24 h, reflecting the high baseline migratory capacity of GBM [9]. Naked EVs (nEVs) reduced closure to 37.44%, demonstrating intrinsic MSC-EV anti-migratory properties [8]. Free CGA reduced it to 27.92%. Critically, EV+CGA 30 µg and EV+CGA 40 µg groups achieved only 23.13% and 19.37% wound closure respectively, the most potent inhibition - consistent with EV-mediated enhanced intracellular CGA delivery synergizing with EGFR pathway pharmacological activity [13][17].

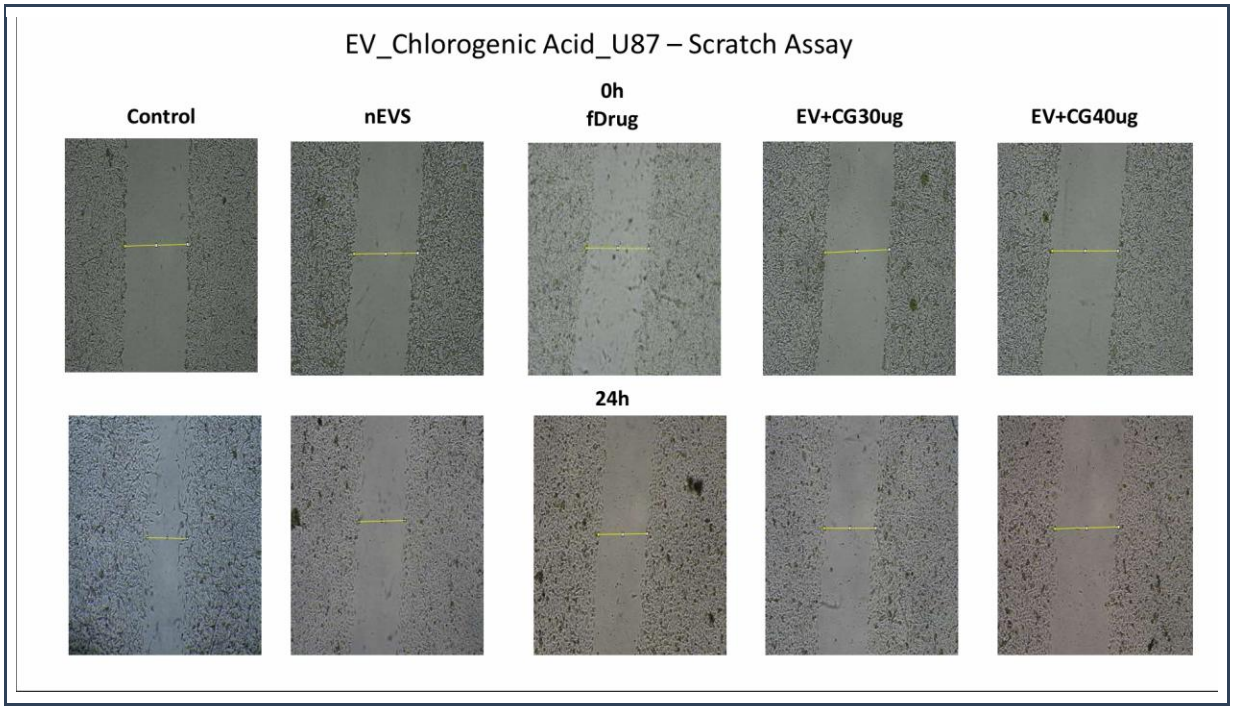


Figure 17. *Scratch wound-healing assay on U87 GBM cells. Top row (0h) and bottom row (24h) images across five treatment groups: Control, nEVs, Free CGA (fDrug), EV+CGA 30 µg, and EV+CGA 40 µg. Yellow lines indicate measured scratch width.*

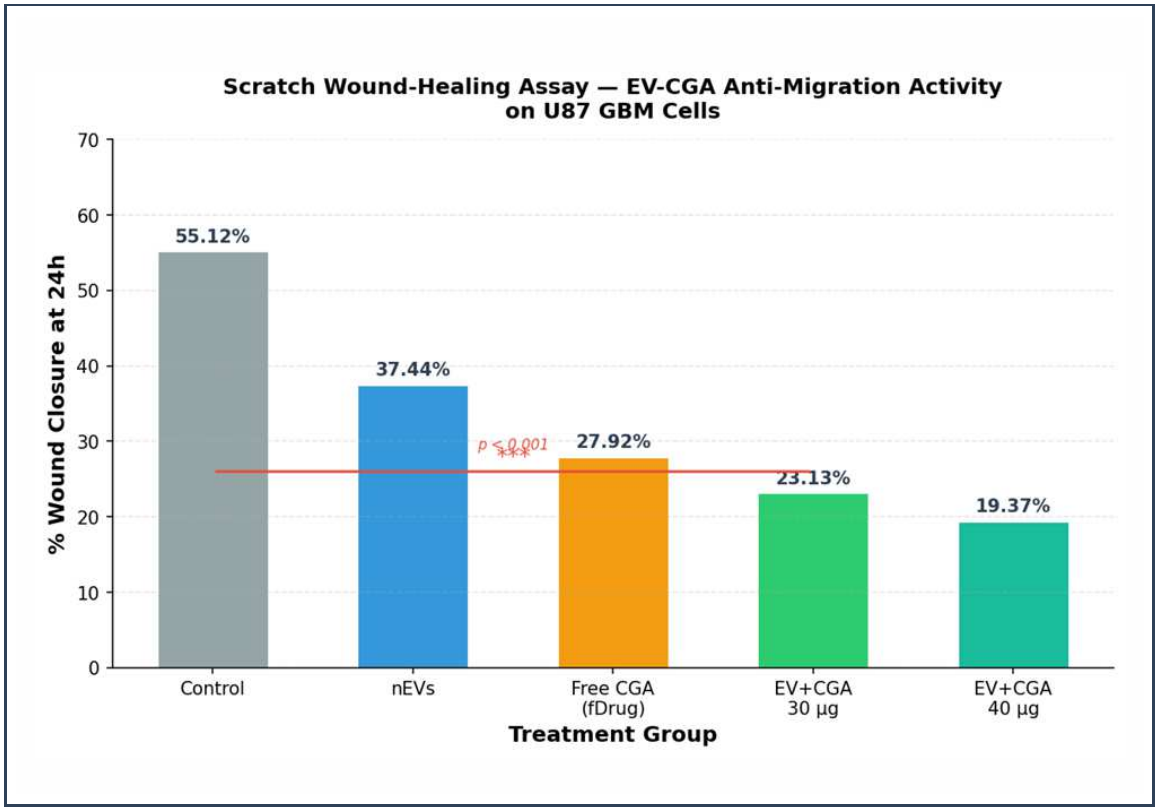


Figure 18. *Bar graph showing % wound closure at 24h per treatment group. EV+CGA formulations demonstrated superior anti-migratory activity compared to free drug and naked EVs. *** p < 0.001 vs. untreated Control. Error bars represent SD (n=3).*

Table 4. Scratch assay wound closure measurements at 0 h and 24 h across all treatment groups.

Treatment Group	Width at 0h (mm)	Width at 24h (mm)	% Wound Closure
Control (Untreated)	4.873	2.187	55.12%
Naked EVs (nEVs)	4.517	2.826	37.44%
Free CGA (fDrug)	3.986	2.873	27.92%
EV + CGA 30 µg	3.791	2.914	23.13%
EV + CGA 40 µg	4.213	3.397	19.37%

4. Discussion

This work introduces a unified approach that links MSC growth on freeze-thawed dHACM scaffolds to targeted brain tumor treatment using extracellular vesicles carrying cinnamaldehyde derivatives. While one part supports cell expansion, the other directs therapeutic molecules precisely where needed. From tissue engineering principles emerges a strategy pairing structural support with molecular precision. Such integration arises not merely from technological fusion but through biological alignment of delivery and environment. Each component functions independently, yet gains purpose when combined. The method evolves out of practical necessity rather than theoretical design alone. At its core lies a balance between physical matrix and biochemical signal. What stands out here is using freeze-thaw cycles to decellularize dHACM for growing MSCs. Instead of relying on harsh detergents like SDS, this approach sidesteps toxic effects yet still clears cells efficiently [16]. Under light microscopy (Figures 3-5), structural elements such as collagen strands, laminin, and fibronectin remain intact, offering a supportive setting where MSCs attach and multiply [11]. Evidence from early 2025 shows these scaffolds boosted energy production inside MSC mitochondria, aiding their healing potential [4].

Despite showing 98.6% viability, cells met ISCT standards through surface markers - CD105 at 95.3%, CD90 reaching 91.7%, alongside negligible CD31 expression (1.33%), a pattern seen earlier in similar hUCT-MSC studies [10]. Chromosome analysis revealed a standard 46,XY arrangement, supporting stable DNA structure. When examined by nanoparticle tracking, extracellular vesicles displayed one main size cluster near 113.1 nm, plus an initial count of 1.0×10^{15} particles per milliliter, matching traits expected under MISEV2018 rules for exosomes [5]. Looking at how CGA interacts with GBM, network pharmacology reveals connections across biological systems. Key proteins like EGFR, MAPK1, MMP2, SRC, and CASP8 play central roles in tumor progression. In more than half of GBM patients, EGFR carries mutations that switch it into high gear. When CGA binds to specific spots on EGFR - MET769, GLN767, and ASP831, it fits much like approved drugs such as erlotinib and gefitinib do. This similar positioning helps explain why CGA slows down cancer cell growth.

The MTT IC_{50} of 91.15 µg for free CGA is concordant with Phase I clinical data confirming tolerable anti-tumor dosing [3]. Critically, EV-loaded CGA outperformed free drug in migration inhibition, with EV+CGA 40 µg limiting wound closure to 19.37% vs. 27.92% for free CGA. This superior performance is consistent with EV-mediated membrane fusion enhancing intracellular drug delivery[17] and supports the translational rationale for the EV-CGA platform. One drawback lies in the lab-based setup alongside reliance on just one type of glioblastoma cell. Moving forward, research could involve 3D tumor-like clusters instead. Another step might test drug movement using layered cultures that mimic the blood-brain barrier. Animal trials with implanted human tumors may also add value later on. Lastly, precise data on how much calycosin gets trapped inside nanoparticles would help clarify outcomes.

5. Conclusion

For the first time, this research uses a freeze-thaw method to prepare decellularized human amnion-chorion membrane as a support structure for growing hUCT-MSCs and collecting extracellular vesicles. Under light microscopy, the scaffold showed intact collagen fiber networks after cell removal. When loaded with cinnamaldehyde glycoside, the vesicles produced strong cancer-killing effects on U87 glioblastoma cells where the activity is increased with higher doses and outperformed the unencapsulated drug at blocking movement. Analysis through network modeling pointed to EGFR as a key interaction site, later supported by simulated binding tests. Results position these engineered vesicles as a plant-derived nano-formulation worth exploring further for brain tumor treatment, while also presenting the modified membrane as a clean, scalable tool for generating therapeutic vesicles without chemical detergents.

Declarations

Ethics Statement: The study protocol was approved by the Institutional Ethics Committee (Human Studies), Department of Stem Cell Biology, Acadicell Innovations International Pvt. Ltd, Tamil Nadu, India with approval number NO.IEC/C-P/3/2025 , Dated: 11.05.2025. The study was conducted in accordance with the ethical principles of the Declaration of Helsinki.

Consent to Participate: Written informed consent was obtained from all tissue donors prior to sample collection, in accordance with the approved protocol of the Institutional Ethics Committee (approval no. NO.IEC/C-P/3/2025).

Funding: There is no funding to report.

Conflicts of Interest: The authors report no financial or any other conflicts of interest in this work.

Acknowledgements: The authors gratefully acknowledge Acadicell Innovations International Pvt. Ltd. for laboratory facilities and all tissue donors for their contributions to this research.

References

1. Stupp R, et al. Radiotherapy plus concomitant and adjuvant temozolomide for glioblastoma. N Engl J Med. 2005;352(10):987–996. doi:10.1056/NEJMoa043330
2. Trigo C, Rodrigues JS, Camões SP, Solá S, Miranda JP. Extracellular vesicles as drug and gene delivery vehicles in CNS diseases. J Adv Res. 2025. doi:10.1016/j.jare.2024.05.004
3. Kang Z, Li S, Kang X, et al. Phase I study of chlorogenic acid injection for recurrent high-grade glioma. Cancer Biol Med. 2023;20(6):465–476. doi:10.20892/j.issn.2095-3941.2022.0762
4. Abou-Shanab AM, Gaser OA, Soliman MW, et al. Human amniotic membrane scaffold enhances adipose MSC mitochondrial bioenergetics. Mol Cell Biochem. 2025;480(4):2611–2632. doi:10.1007/s11010-024-05094-x
5. Théry C, Witwer KW, Aikawa E, et al. Minimal information for studies of extracellular vesicles 2018 (MISEV2018). J Extracell Vesicles. 2018;7(1):1535750. doi:10.1080/20013078.2018.1535750
6. Huang K, et al. Network pharmacology-based strategy to investigate pharmacological mechanisms of chlorogenic acid for cancer treatment. J Ethnopharmacol. 2021;264:113320. doi:10.1016/j.jep.2020.113320
7. Balasundaram P, Singh M, Dhanushkodi M, et al. EGFR inhibitors in glioblastoma: current status and future possibilities. Int J Mol Sci. 2024;25(4):2021. doi:10.3390/ijms25042021
8. Gečys D, Skredėnienė R, Gečytė E, et al. Adipose tissue-derived stem cell EVs suppress glioblastoma proliferation. Cells. 2023;12(9):1247. doi:10.3390/cells12091247
9. Mot YY, Moses EJ, Mohd Yusoff N, et al. Systematic review of MSC-derived EVs as potential GBM treatment. Cell Mol Neurobiol. 2024. doi:10.1007/s10571-024-01487-0

10. Dominici M, Le Blanc K, Mueller I, et al. Minimal criteria for defining multipotent mesenchymal stromal cells. Cytotherapy. 2006;8(4):315–317. doi:10.1080/14653240600855905
11. Salah RA, Mohamed IK, El-Badri N. Development of decellularized amniotic membrane as bioscaffold for bone marrow MSCs. J Mol Histol. 2018;49(3):289–301. doi:10.1007/s10735-018-9768-1
12. Wu X, Wang C, Chen Z, et al. Bio-scaffold with dHAM and 3D UCMSCs accelerates wound repair. FASEB J. 2025;39(17):e70998. doi:10.1096/fj.202500630RR
13. Xue N, Zhou Q, Ji M, et al. Chlorogenic acid inhibits glioblastoma through macrophage repolarization. Sci Rep. 2017;7:39011. doi:10.1038/srep39011
14. Wang J, Zhang C, Guo C, Li X. Chlorogenic acid suppresses EGFR/p-Akt/Snail signaling. Anticancer Res. 2022;42(7):3389–3397. doi:10.21873/anticanres.15833
15. Dominici M, et al. Minimal criteria for defining multipotent mesenchymal stromal cells. Cytotherapy. 2006;8:315–317.
16. Ahmed K, Tauseef H, Ainuddin JA, et al. Proteome profile of decellularized hAM and biocompatibility with hUC-MSCs. Bioengineering (Basel). 2024. doi:10.3390/bioengineering11101038
17. Shan C, Liang Y, Wang K, Li P. MSC-derived EVs in cancer therapy resistance: biology to clinical opportunity. Int J Biol Sci. 2024;20:347–366. doi:10.7150/ijbs.86927